Applied Acoustics 235 (2025) 110676

Contents lists available at ScienceDirect

Applied Acoustics

journal homepage: www.elsevier.com/locate/apacoust

Broadband sound reduction in space-coiling ventilation structures with microperforated shells

Yonghui Zhang, Lei Zhang, Youdong Duan, Xiaoming Zhou *

Key Laboratory of Dynamics and Control of Flight Vehicle of Ministry of Education, School of Aerospace Engineering, Beijing Institute of Technology, Beijing, 100081, China

ARTICLE INFO

Keywords:
Sound reduction
Sound absorption
Air ventilation
Microperforated panels

ABSTRACT

Ventilation structures supported by the Fano-like interference can act as high-performance sound silencers, yet the bandwidth gets limited eventually by coexisting resonant transmission. In this work, we focus on the space-coiling ventilation structure, and overcome the limitation by introducing a cylindrical shell made of microperforated panels (MPPs) in between the channel and ventilation pipe. The underlying mechanism is due to the resonance-induced field intensity enhancement within coiling channels, which can produce a significant pressure difference on both sides of the MPP to damp resonant acoustic transmission. Based on this behavior, broadband sound reduction with the bandwidth exceeding an octave can be achieved when two such structural elements are cascaded. Enhanced acoustic damping by MPPs and broadband sound reduction in bi-cell structures are numerically analyzed and validated experimentally.

1. Introduction

Recently, there is a growing interest in achieving broadband sound attenuation by structured materials with air ventilation. Ventilation sound barriers can be configured via sonic crystals with the periodical arrangement of cell structures to block sounds by Bragg or local-resonance scatterings [1,2]. Another widely explored model consists of a duct or pipe with side-loaded or embedded structures for either sound absorption or reflection [3–5]. The ducts with side Helmholtz or Fabry-Pérot resonators, also known as duct silencers, can dissipate sounds in narrow bands near resonant frequencies [6–8]. By assembling multiple element structures, a broadband absorption and attenuation for sounds can be achieved [9,10]. The duct silencer allows a high-efficiency air ventilation, yet the side branch occupies an additional expansion volume outside of the duct, which is bulky at low operation frequencies.

The model with absorptive resonators embedded within the duct is required in some practical applications [11–15]. There is a trade-off between the ventilation efficiency and noise reduction bandwidth for this duct-borne model. A simple yet efficient configuration is to couple a space-coiling channel with a straight one, which can produce a low-transmission band due to the Fano resonance [16–19]. The synergy of mode superposition and Fano resonances can yield an enhancement of operation bandwidth up to half an octave [20]. It becomes challenging to further broaden the isolation band as there always exists the resonance-induced high transmission outside of the sound transmission valley.

Microperforated panel (MPP) is an essential structured material widely used for sound absorption and attenuation. MPPs can be employed for noise reduction control in various circumstances. The MPP with a backing cavity can act as the resonance-type sound absorber. Low-frequency sound absorption can be improved by coupling the MPP with the coiled-up channel [21] or Helmholtz resonator [22]. Absorption bandwidth can be enhanced in a double-layer MPP system with parallel or cascading arrangements [23–25]. Sound isolation performance of expansion chambers can be improved by the built-in MPP [26]. The cavity-backed MPPs facing the duct wall can absorb sounds from the grazing direction [27–29]. Flat MPPs rolled into a cylindrical shell can act as the unit cell of sonic crystals for acoustic attenuation [30–32]. MPPs can be also used to suppress the interior resonance response of acoustic enclosure systems [33,34].

In this work, we propose to suppress the resonant transmission of in-duct space-coiling structures by introducing a cylindrical MPP shell, which is added in between the coiling channel and straight one. Sound absorption at resonant frequencies can be enhanced with the presence of MPPs, leading to the reduction of resonant transmission, as will be validated numerically and experimentally. It is further found that broad-

* Corresponding author.
E-mail address: zhxming@bit.edu.cn (X. Zhou).

https://doi.org/10.1016/j.apacoust.2025.110676
Received 25 September 2024; Received in revised form 13 December 2024; Accepted 8 March 2025

Available online 14 March 2025
0003-682X/© 2025 Elsevier Ltd. All rights are reserved, including those for text and data mining, AI training, and similar technologies.

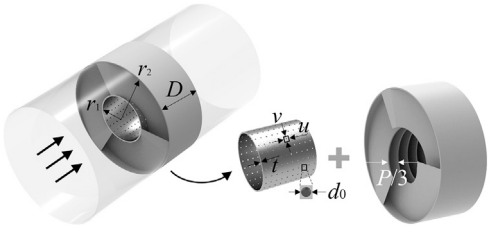

Fig. 1. Schematic illustration of the proposed ventilation structure consisting of three helical channels coiled up around a straight pipe subject to a plane wave incidence, where the MPP shell is placed between the helical channel and straight pipe.

band sound reduction can be realized when two such structural elements are cascaded. The influences of structural parameters on the sound isolation behavior are analyzed to reveal the superior performance of the MPP-assisted structure.

2. Model and results

2.1. Ventilated structures with MPP shells

The ventilation structure consists of three helical channels coiled up around a straight pipe, where a micro-perforated cylindrical shell is placed between the channel and pipe, as shown in Fig. 1. Adjacent helical channels are separated by a spiral blade with the geometry defined by $x = r\cos(\psi)$, $y = r\sin(\psi)$, and $z = \psi P/(2\pi)$, $r \in [r_1, r_2]$, and $\psi \in [0, 2\pi D/P]$, where D and P are respectively the thickness and pitch of the helical channel, and r_1, r_2 refers to its inner and outer radius. The cylindrical shell is made of the MPP of thickness t, where arrays of submillimetric orifices of diameter d_0 are distributed in a square lattice of periodicity u and v with the porosity $\sigma = \pi d_0^2/(4uv)$.

Consider a plane acoustic wave normally incident on the ventilation structure. Geometric parameters are chosen as $r_1 = 20$ mm, $r_2 = 50$ mm, $D = 40$ mm, $P = 35$ mm for the helical channel, and $t = 1$ mm, $d_0 = 0.17$ mm, $u = 1.9$ mm, $v = 1.85$ mm for the MPP shell, which yields the porosity $\sigma = 0.65\%$. Numerical simulation is based on the pressure acoustics module of the finite element software COMSOL Multiphysics. The cylindrical surface of the waveguide system is set as the hard boundary, and two end ports are terminated by the non-reflection boundary. The structure system is meshed with the tetrahedral element, and the maximum size of elements is less than 1/20 of the minimum wavelength. The MPP is modeled by an acoustic impedance with the formula proposed by Maa [35]

$$Z = \frac{32\mu t}{\sigma d_0^2}\left(1 + \frac{x^2}{32}\right)^{1/2} + i\omega\rho_0 t\left[1 + \left(9 + \frac{x^2}{2}\right)^{-1/2}\right] \quad (1)$$

where $\mu = 1.81 \times 10^{-5}$ Pa·s is the air dynamic viscosity, ω is the angular frequency, i is the imaginary unit, and $x = d_0\sqrt{\rho_0\omega/\mu}/2$. The density ρ_0 and sound velocity c_0 are taken as 1.21 kg/m^3 and 343 m/s, respectively. Assume that the channel and pipe are free of air viscous loss to evaluate purely the impact of the MPP damping performance. Fig. 2(a) shows by the dashed line the simulation result of acoustic energy transmission of the unperforated structure. The Fano-like interference can lead to the low-transmission phenomenon in a finite band, which has been widely exploited to design sound insulation structures [36–38]. However, the band is sandwiched between two transmission peaks at 845 Hz and 1720 Hz, which defines the range of operation frequencies for sound isolation. Further broadening of the sound isolation bandwidth requires the suppression of resonant transmission. High transmission at these two frequencies arises from the dipole and monopole resonances of the helical structure, and results in the significant pressure difference between the coiling channel and straight pipe, as seen in the inset of Fig. 2(a). Based on this observation, we replace the cylindrical

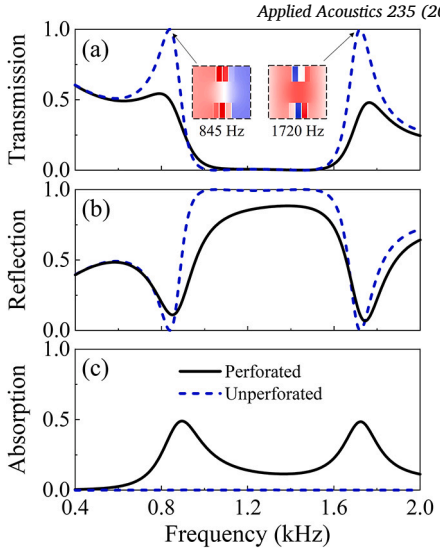

Fig. 2. (a) Acoustic energy transmission, (b) reflection and (c) absorption of ventilation structures in both perforated and unperforated cases.

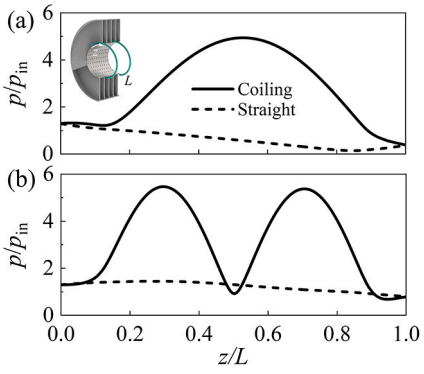

Fig. 3. Normalized acoustic pressure amplitude on the coiling-channel and straight-pipe sides of the MPP along the helical paths at frequencies (a) 895 Hz and (b) 1725 Hz.

shell with the MPP, which could be fully activated by the pressure gradient to absorb impinging sounds. This is the basic idea of the proposed structure to suppress the resonant transmission.

Figs. 2(a-c) show by the solid line acoustic energy transmission, reflection and absorption of the ventilation structure equipped with the MPP shell, respectively. Due to the action of MPPs, acoustic absorption at resonant frequencies can be significantly enhanced, leading to the reduction of resonant transmission. To verify the working mechanism of the MPP shell, Figs. 3(a, b) show the pressure amplitude distribution (normalized with respect to the incident one) on both sides of the MPP along the helical paths at frequencies 895 Hz and 1725 Hz, respectively. The field distribution is nearly uniform in the straight pipe region, while an enhancement of pressure amplitudes due to the resonance effect can be observed within the coiling channel. As a result, a high pressure contrast across the shell is formed and induces the air friction loss in micro holes for sound damping.

2.2. Experimental analyses

In experiment, the coiling-channel structure is fabricated using Acrylonitrile Butadiene Styrene (ABS) by 3D printing. The MPP shell is made of the SUS304 steel plate with cores punched by laser processing. The sample is installed by assembling the channel structure and MPP shell, as shown in Fig. 4(a). The model structure without micro holes is also fabricated by 3D printing for comparison study. Acoustic properties are measured by the Brüel & Kjær 4206T impedance tube system. Figs. 4(b-

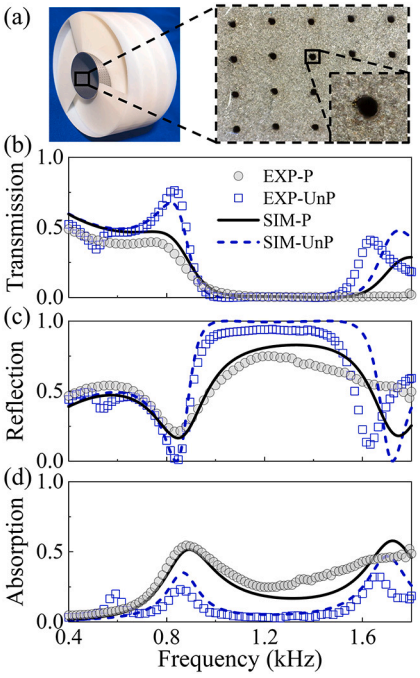

Fig. 4. (a) Photograph of the fabricated sample with the MPP shell; Simulation and experimental results of (b) acoustic energy transmission, (c) reflection and (d) absorption of the coiling-channel structure with and without MPP shells.

d) show respectively the measured sound transmission, reflection and absorption for the model system studied in Fig. 2. Experimental results disclose that there exists inherent sound damping within channeling structures, which arises from the thermoviscous loss due to the narrow-channel effect. In numerical simulations, this intrinsic damping is modeled by involving the complex sound velocity $343(1+0.02i)$ m/s in the air domain. The simulation results are presented in Fig. 4(b-d), and show a good agreement with experimental results. In the presence of the MPP, the damping performance is strengthened near resonant frequencies, and causes the significant reduction of resonant sound transmission. The magnitude and frequency bandwidth of sound reduction can be further improved when two such cell structures are coupled as demonstrated later.

Air flow measurement in a cylindrical waveguide is conducted to assess the ventilation performance of the sample structure as shown in Fig. 5(a). An electric fan is placed at the inlet port of the waveguide to provide a stable wind flow. The air flow velocity at the outlet is measured by an anemometer for samples with and without MPP shells, which are positioned in the central region of the waveguide. The wind velocity data in the absence and presence of the sample are recorded by taking the average of five times repeated measurements. Fig. 5(b) shows the ratio between the outlet wind speed of the sample and that of the empty waveguide, which characterizes the ventilation performance. The velocity ratio is 16.4% for the MPP structure, close to the percentage of opening 14.4% for the straight channel, and is slightly lower than the velocity ratio 17.2% of the unperforated structure, indicating that the MPP shell has a weak influence over the ventilation performance.

2.3. Broadband sound reduction in bi-cell structures

Consider a composite structure made by cascading two cell structures with a separation W, as sketched in Fig. 6(a). One cell structure is same to the model in Fig. 2 with the helical pitch $P_1 = 35$ mm, and the corresponding sound transmission loss (STL) result is replotted in Fig. 6(b). The transmission reduction is up to 10 dB in the frequency range from 958 Hz to 1635 Hz. Another cell structure is designed by just modifying the helical pitch as $P = 23$ mm while maintaining other parameters

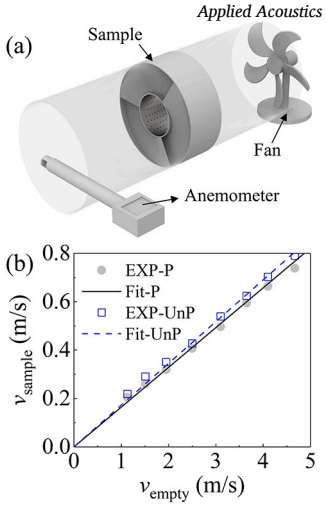

Fig. 5. (a) Schematic diagram of the setup to measure the air flow performance; (b) The measured wind speeds with and without the sample and their fitting results.

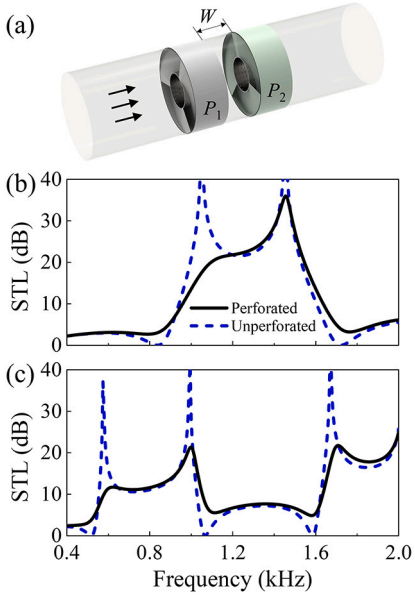

Fig. 6. (a) Schematic of the bi-cell structure; Sound transmission loss (STL) of single cell structures with different pitch parameters (b) $P_1 = 35$ mm and (c) $P_2 = 23$ mm in both perforated and unperforated cases.

unchanged. This would lead to the shifting of sound isolation band as shown in Fig. 6(c), where the STL exceeds 10 dB in the bands of 580-1055 Hz and 1632-2000 Hz. By choosing the separation $W = 40$ mm, Fig. 7 shows the simulation results of STL, sound reflection and absorption of the bi-cell structure in both perforated and unperforated cases, where the thermoviscous damping within channels is not taken into account. The MPP shell is found to play a central role in reducing acoustic resonant transmission near 904 Hz and 1590 Hz, realizing a broadband sound isolation at frequencies from 941 Hz to 2000 Hz with the STL over 20 dB.

To disclose the working mechanism of the MPP shell, Figs. 7(d, e) illustrate the pressure amplitude distributions at frequencies 904 Hz and 1590 Hz, respectively. In the unperforated case, it is seen that high transmission at 904 Hz is caused by the inter-cell resonance, where a high intensity sound field is localized in the region between two cells. When the micro holes are added to the shell, sound energy is dissipated to induce a high sound absorption as seen in Fig. 7(c). This damping behavior can weaken the coupling resonance, and enhance the transmission loss.

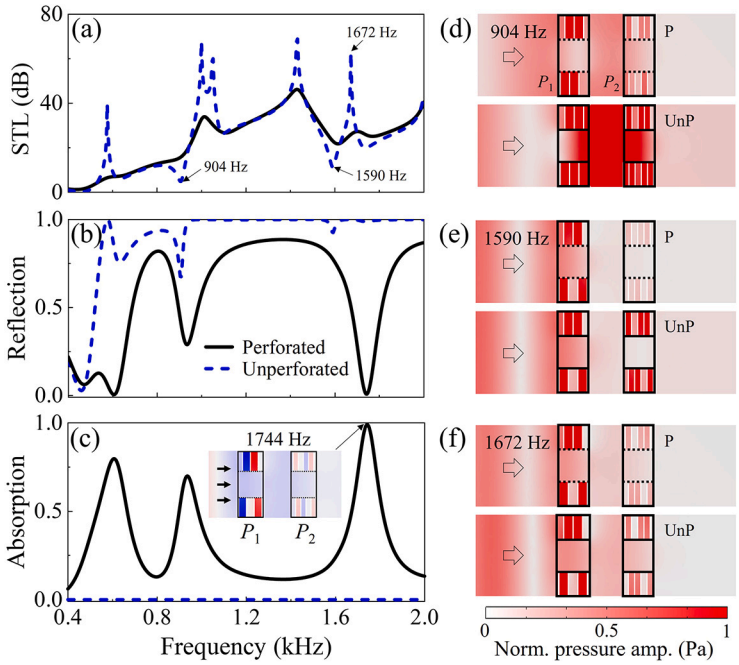

Fig. 7. Simulation results of (a) STL, (b) reflection and (c) absorption coefficients of the bi-cell structure in both perforated (P) and unperforated (UnP) cases where the thermoviscous damping within channels is not taken into account; Pressure amplitude distributions at frequencies (d) 904 Hz, (e) 1590 Hz, and (f) 1672 Hz.

By contrast, the high transmission at 1590 Hz is due to the intra-cell resonance as observed in Fig. 7(e), where sound energy is localized primarily inside helical channels. Thereby, the MPP shell can significantly affect the resonant behavior with the result of the flattening of the STL spectrum. In Fig. 7(c), we can also observe a nearly perfect sound absorption at around 1744 Hz. According to Figs. 6(b, c), the cell structure with P_1 is characterized by the resonant effect near this frequency, while the structure with P_2 has a high sound reflection. When two cell structures are combined together, the structure with P_2 serves as the sound blocking wall such that the waveguide structure behaves like the one-port system. Assisted by the resonant behavior, the MPP in the structure with P_1 can be fully activated to damp sounds as evidenced by the pressure distribution in the inset of Fig. 7(c), thus leading to the high sound absorption at frequency 1744 Hz. On the other hand, we also examine the weak transmission for the anti-resonance frequency 1672 Hz, at which the field distribution is shown in Fig. 7(f). Although the anti-resonance behavior is weakened by the MPP damping, the high STL can still be achieved near this frequency due to the joint action of sound absorption and reflection.

Experiments are performed to evaluate acoustic performance of the bi-cell structure. Figs. 8(a-c) show respectively experimental results of the STL, reflection and absorption of the bi-cell structure with and without MPP shells. Numerical simulations that account for the inherent damping are also performed, and the results are in accordance with experimental ones. Notice that simulation results predict a high absorption peak at around 1750 Hz, but deviate from the experimental results. A potential reason for the discrepancy is that the Maa's impedance model [35] used in the simulation for characterizing the MPP structure may not be accurate at relatively high frequencies above 1.5 kHz due to the near-field effect caused by shorter wavelengths, damping effect within the channels, and complex acoustic coupling across different length scales. In experiment, the bi-cell structure with the MPP exhibits the flattened absorption peak near resonant frequencies and the enhanced absorption at non-resonant frequencies, which are signatures of heavily damped systems. In addition, there is a considerable reflection of sound energy in the broad frequency range. As a result, a wideband sound reduction with the STL over 20 dB can be achieved at frequencies from 894 Hz to 1800 Hz with the bandwidth exceeding an octave, which is superior to the unperforated structure.

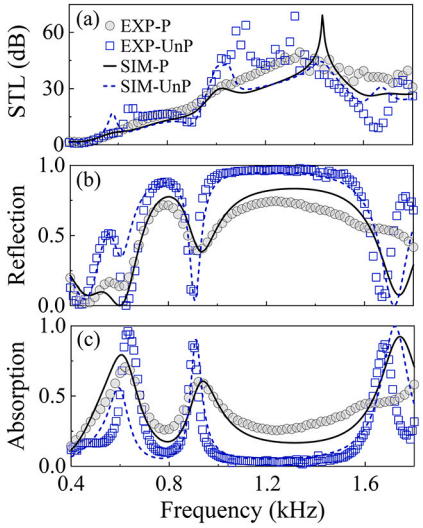

Fig. 8. Simulation and experimental results of (a) STL, (b) reflection and (c) absorption coefficients of the bi-cell structure in both perforated (P) and unperforated (UnP) cases where the thermoviscous damping within channels is taken into account in numerical simulation.

2.4. The influence of structural parameters

Parametric analyses are conducted below to illustrate the effect of the cell spacing W, incident angle θ, and MPP parameters (core diameter d_0 and porosity σ) based on numerical simulations that account for the intrinsic damping. Fig. 9(a) shows the spectrum of transmission reduction for different W, where the contour line of 20 dB is drawn to display the variation of the isolation bandwidth. Broadband reduction of sound transmission can be achieved in a moderate region of W from 10 mm to 70 mm. The high STL in a wide frequency band is caused by the strong reflection, and the MPP structure plays an important role in improving sound isolation at band-edge frequencies where acoustic reflection becomes weak, as shown in Figs. 9(c, e).

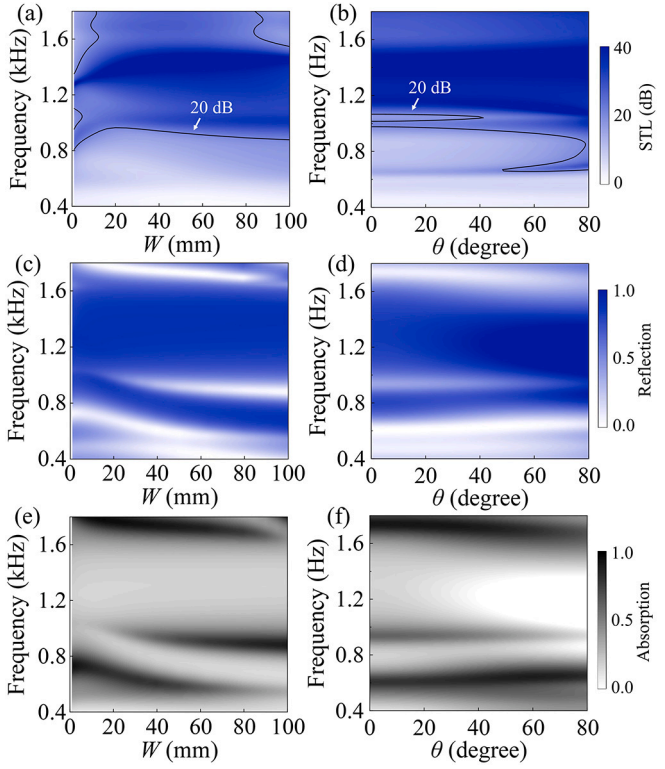

Fig. 9. (a) The STL, (c) sound reflection and (e) absorption spectra for various cell spacing W; (b, d, f) The corresponding results for different incident angle θ.

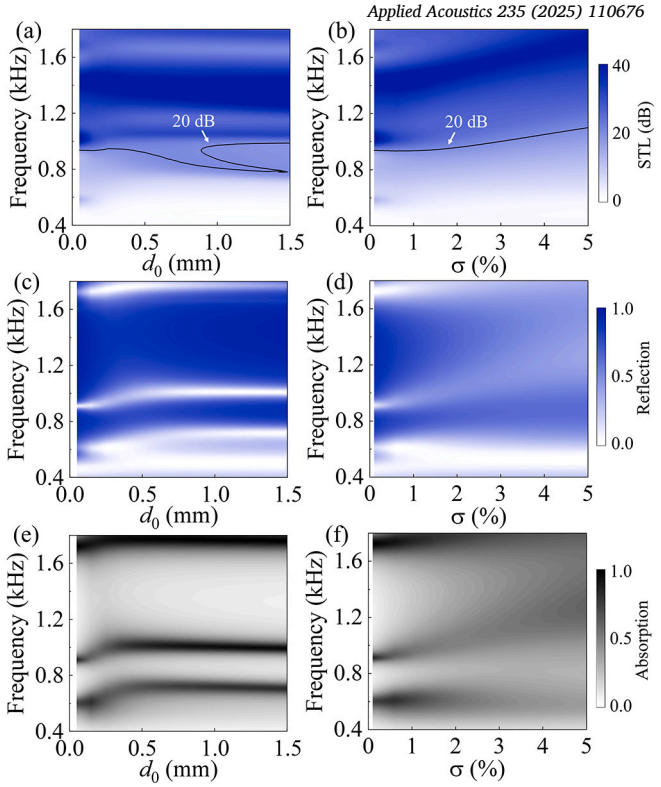

Fig. 10. (a) The STL, (c) sound reflection and (e) absorption spectra for various core diameter d_0; (b, d, f) The corresponding results for various core porosity σ.

Sound barriers are not just subject to normal incidence in practical applications. Here, the sound blockage effect is studied in situations where a plane acoustic wave impinges the bi-cell structure at an oblique angle θ. Figs. 9(b, d, f) show respectively the STL, sound reflection and absorption spectra for the incident angle θ changing from 0° to 80°. The broadband behavior of sound isolation can be maintained, and the bandwidth has even been widened as θ increases. This is mostly because of the enlarged impedance contrasts at large θ, which result in the enhanced reflection in spite of the decrease of sound absorption.

Finally analyze the influence of two key MPP parameters, i.e., the core diameter and porosity. Fig. 10 shows the STL, sound reflection and absorption spectra against the variation of the core diameter d_0 and porosity σ. Notice that the core diameter $d_0 = 0.17$ mm is fixed when the porosity σ is examined. Sound absorption results demonstrate the heavily damped nature at specific frequencies across a broad parameter range of d_0 and σ. By compensating for the weak sound reflection, this damping performance is crucial to the broadband sound attenuation, as displayed in Figs. 10(a, b).

3. Conclusions

Ventilation silencing structures consisting of helical channels coiled around a straight pipe with a MPP shell separation are proposed. The space-coiling structure supports a transmission valley because of the Fano-like interference, meanwhile the coexisting resonant acoustic transmission can be efficiently damped by the MPP shell, thus lifting the restriction to further broaden the isolation bandwidth. Based on this behavior, two cell structures are coupled with the combined transmission valleys to acquire broadband sound reduction as validated numerically and experimentally. The sound transmission loss is over 20 dB in the frequency range 894-1800 Hz, superior to the unperforated system. Based on numerical simulations, the effects of the cell spacing, incident angle, and MPP parameters are analyzed to demonstrate the good sound isolation performance of the bi-cell structure. It is worth to note that the non-local coupling is recently demonstrated to provide new degrees of freedom for the broadband acoustic control [39]. In our study, the MPP provides the coupling between the coiling and straight channels, and can be considered as the non-local interaction with strong damping. These studies highlight the importance of the non-local coupling in the design of broadband acoustic structures. The proposed model holds application potentials for duct-borne sound control in civil, transportation, and industrial engineering.

CRediT authorship contribution statement

Yonghui Zhang: Writing – original draft, Methodology, Investigation, Conceptualization. **Lei Zhang:** Validation, Investigation. **Youdong Duan:** Validation, Investigation. **Xiaoming Zhou:** Writing – review & editing, Supervision, Methodology, Investigation, Conceptualization.

Declaration of competing interest

The authors declare that they have no known competing financial interests or personal relationships that could have appeared to influence the work reported in this paper.

Acknowledgement

This work was supported by the National Natural Science Foundation of China (12225203, 11622215, 11872111, 11991030, and 11991033) and the 111 Project (B16003).

Data availability

Data will be made available on request.

References

[1] Wu X, Au KY, Yeung, Li X, Roberts RC, Tian J, Hu C, et al. High-efficiency ventilated metamaterial absorber at low frequency. Appl Phys Lett 2018;112(10):103505. https://doi.org/10.1063/1.5025114.

[2] Xu Z, Gao H, Ding Y, Yang J, Liang B, Cheng J. Topology-optimized omnidirectional broadband acoustic ventilation barrier. Phys Rev Appl 2020;14(5):054016. https://doi.org/10.1103/PhysRevApplied.14.054016.

[3] Gao C, Hu C, Hou B, Zhang X, Li S, Wen W. Ventilation duct silencer design for broad low-frequency sound absorption. Appl Acoust 2023;206:109324. https://doi.org/10.1016/j.apacoust.2023.109324.

[4] Crivoi A, Du L, Fan Z. Ventilated acoustic meta-barrier based on layered Helmholtz resonators. Appl Acoust 2023;205:109263. https://doi.org/10.1016/j.apacoust.2023.109263.

[5] Yu Y, Jia H, Yang Y, Zhao H, Shi Q, Kong P, et al. Multi-order resonators for acoustic multiband asymmetric absorption and reflection. J Appl Phys 2022;131(13). https://doi.org/10.1063/5.0084450.

[6] Meng Y, Romero-García V, Gabard G, Groby J, Bricault C, Goudé S. Subwavelength broadband perfect absorption for unidimensional open-duct problems. Adv Mater Technol 2023:2201909. https://doi.org/10.1002/admt.202201909.

[7] Liu X, Duan M, Liu M, Xin F, Zhang C. Acoustic labyrinthine porous metamaterials for subwavelength low-frequency sound absorption. J Appl Phys 2021;129(19). https://doi.org/10.1063/5.0032045.

[8] Xiang X, Wu X, Li X, Wu P, He H, Mu Q, et al. Ultra-open ventilated metamaterial absorbers for sound-silencing applications in environment with free air flows. Extrem Mech Lett 2020;39:100786. https://doi.org/10.1016/j.eml.2020.100786.

[9] Wang TM, Gong C, Zhang SY, Zhu YZ, Long HY, Cheng Y, et al. An acoustic metaliner for ultra-broadband sound absorption. Appl Phys Lett 2023;123(16):161704. https://doi.org/10.1063/5.0166720.

[10] Nguyen H, Wu Q, Xu XC, Chen H, Tracy S, Huang G. Broadband acoustic silencer with ventilation based on slit-type Helmholtz resonators. Appl Phys Lett 2020;117(13):134103. https://doi.org/10.1063/5.0024018.

[11] Romero-García V, Jiménez N, Groby JP, Merkel A, Tournat V, Theocharis G, et al. Perfect absorption in mirror-symmetric acoustic metascreens. Phys Rev Appl 2020;14(5):054055. https://doi.org/10.1103/PhysRevApplied.14.054055.

[12] Xiao Z, Gao P, Wang D, He X, Wu L. Ventilated metamaterials for broadband sound insulation and tunable transmission at low frequency. Extrem Mech Lett 2021;46:101348. https://doi.org/10.1016/j.eml.2021.101348.

[13] Lin DK, Xiao XW, Yang CC, Ho S, Chou LC, Chiang CH, et al. An acoustic impedance design method for tubular structures with broadband sound insulations and efficient air ventilation. Appl Acoust 2024;220:109983. https://doi.org/10.1016/j.apacoust.2024.109983.

[14] Crivoi A, Fan Z. Noise attenuating performance of metasurfaces with regular Euclidean tiling and uniformly embedded Helmholtz resonators. Appl Acoust 2022;185:108388. https://doi.org/10.1016/j.apacoust.2021.108388.

[15] Yuan X, Li Q, Wu C, Huang Y, Wu X. Broadband ventilated metamaterial absorber from non-local coupling. Extrem Mech Lett 2024;66:102119. https://doi.org/10.1016/j.eml.2023.102119.

[16] Sun M, Fang XS, Mao DX, Wang X, Li Y. Broadband acoustic ventilation barriers. Phys Rev Appl 2020;13(4):44028. https://doi.org/10.1103/PhysRevApplied.13.044028.

[17] Ghaffarivardavagh R, Nikolajczyk J, Anderson S, Zhang X. Ultra-open acoustic metamaterial silencer based on Fano-like interference. Phys Rev B 2019;99(2):24302. https://doi.org/10.1103/PhysRevB.99.024302.

[18] Kumar S, Lee HP. Labyrinthine acoustic metastructures enabling broadband sound absorption and ventilation. Appl Phys Lett 2020;116(13). https://doi.org/10.1063/5.0004520.

[19] Yang J, Lee JS, Lee HR, Kang YJ, Kim YY. Slow-wave metamaterial open panels for efficient reduction of low-frequency sound transmission. Appl Phys Lett 2018;112(9). https://doi.org/10.1063/1.5003455.

[20] Tang Y, Liang B, Lin S. Broadband ventilated meta-barrier based on the synergy of mode superposition and consecutive Fano resonances. J Acoust Soc Am 2022;152(4):2412–8. https://doi.org/10.1121/10.0014911.

[21] Li Y, Yan J. Acoustic transmission characteristics based on coiled-up space metamaterials. Appl Acoust 2023;203. https://doi.org/10.1016/j.apacoust.2022.109199.

[22] Mahesh K, Mini RS. Theoretical investigation on the acoustic performance of Helmholtz resonator integrated microperforated panel absorber. Appl Acoust 2021;178:108012. https://doi.org/10.1016/j.apacoust.2021.108012.

[23] Zhao L, Lin TR. A turned double-layer microperforated panel for low frequency sound absorption in enclosures with limited cavity space. Appl Acoust 2022;188. https://doi.org/10.1016/j.apacoust.2021.108594.

[24] Mosa AI, Putra A, Ramlan R, Esraa A-A. Wideband sound absorption of a double-layer microperforated panel with inhomogeneous perforation. Appl Acoust 2020;161. https://doi.org/10.1016/j.apacoust.2019.107167.

[25] Boccaccio M, Bucciarelli F, Fierro GPM, Meo M. Microperforated panel and deep subwavelength Archimedean-inspired spiral cavities for multi-tonal and broadband sound absorption. Appl Acoust 2021;176. https://doi.org/10.1016/j.apacoust.2020.107901.

[26] Gai X, Xing T, Kang Z, Li X, Zhang B, Cai Z, et al. Study on sound insulation performance of the periodic arrangement expansion chambers structure with built-in micro-perforated panel. Appl Acoust 2020;161:107187. https://doi.org/10.1016/j.apacoust.2019.107187.

[27] Kim DY, Ih JG. Wideband reduction of in-duct noise using acoustic metamaterial with serially connected resonators made with mpp and cavities. Appl Phys Lett 2020;116(25). https://doi.org/10.1063/5.0011558.

[28] Zhang X, Cheng L, Liu Y, Du J. Acoustic modelling and analyses of geometrically complex systems with micro-perforated panels. J Sound Vib 2021;499:115995. https://doi.org/10.1016/j.jsv.2021.115995.

[29] Yang C, Xu H. Effects of the backing cavity on the acoustic absorption of a microperforated panel absorber. Appl Acoust 2020;166. https://doi.org/10.1016/j.apacoust.2020.107361.

[30] García-Chocano VM, Cabrera S, Sánchez-Dehesa J. Broadband sound absorption by lattices of microperforated cylindrical shells. Appl Phys Lett 2012;101(18):184101. https://doi.org/10.1063/1.4764560.

[31] Chen JJ, Zhang YH, Yu YK, Zhai Y, Nguyen H, Tracy S, et al. Broadband acoustic attenuation in microperforated meta-shells with ventilation. Appl Phys Lett 2023;122(23):231701. https://doi.org/10.1063/5.0152725.

[32] van der Aa B, Forssén J. Scattering by an array of perforated cylinders with a porous core. J Acoust Soc Am 2014;136(5):2370–80. https://doi.org/10.1121/1.4896566.

[33] Yang C, Cheng L. Sound absorption of microperforated panels inside compact acoustic enclosures. J Sound Vib 2016;360:140–55. https://doi.org/10.1016/j.jsv.2015.09.024.

[34] Liu MY, Zhou XM. Sound reduction control in acoustic enclosure with air ventilation. Acta Mech Solida Sin 2023;36(6):763–9. https://doi.org/10.1007/s10338-023-00423-x.

[35] Maa D-Y. Potential of microperforated panel absorber. J Acoust Soc Am 1998;104(5):2861–6.

[36] Chen A, Zhao X, Yang Z, Anderson S, Zhang X. Broadband labyrinthine acoustic insulator. Phys Rev Appl 2022;18(6):64057. https://doi.org/10.1103/PhysRevApplied.18.064057.

[37] Xiang L, Wang G, Zhu C, Shi M, Hu J, Luo G. Ventilation barrier with space-coiling channels of varying cross-section for broadband sound insulation. Appl Acoust 2022;201:109110. https://doi.org/10.1016/j.apacoust.2022.109110.

[38] Li X, Zhang H, Tian H, Huang Y, Wang L. Frequency-tunable sound insulation via a reconfigurable and ventilated acoustic metamaterial. Appl Acoust 2022;55(49):495108. https://doi.org/10.1088/1361-6463/ac9985.

[39] Zhu Y, Dong R, Mao D, Wang X, Li Y. Nonlocal ventilating metasurfaces. Rev Phys Appl 2023;19(1):014067. https://doi.org/10.1103/PhysRevApplied.19.014067.